Materials Science & Engineering A 848 (2022) 143393

Contents lists available at ScienceDirect

Materials Science & Engineering A

journal homepage: www.elsevier.com/locate/msea

Heterostructure alleviates Lüders deformation of ultrafine-grained stainless steels

Guosheng Sun [a,1], Jizi Liu [a,b,*,1], Yuntian Zhu [c,d,**]

[a] Nano and Heterogeneous Materials Center, School of Materials Science and Engineering, Nanjing University of Science and Technology, Nanjing, 210094, People's Republic of China

[b] Materials Analysis and Test Center, Nanjing University of Science and Technology, Nanjing, 210094, People's Republic of China

[c] Department of Materials Science & Engineering, City University of Hong Kong, Kowloon, 999077, Hong Kong, People's Republic of China

[d] Mechanical Behavior Division of Shenyang National Laboratory for Materials Science, City University of Hong Kong, Kowloon, 999077, Hong Kong, People's Republic of China

ARTICLE INFO

Keywords:
Stainless steel
Heterostructure
Lüders band
Strain delocalization
HDI hardening

ABSTRACT

Ultrafine-grained (UFG) 304 stainless steel is much stronger than its coarse-grained counterpart. However, it develops undesired Lüders bands during deformation. Here we report a bi-modal heterostructure that can effectively suppress Lüders deformation in the UFG 304 stainless steel, which produces a strong strain hardening to improve the ductility and toughness, without sacrificing much strength. These superior mechanical properties are attributed to strain delocalization capability of the bi-modal heterostructure, which results in lower stress concentration and consequently postpones the martensitic transformation.

1. Introduction

Homogenously refining grains into ultrafine and nanometer scale can generally make materials several times stronger, but this sacrifices the ductility, due to a dramatic loss of work-hardening capability and significant strain localization. The Lüders deformation is characterized with yield drop on the stress-strain curve and a stress plateau due to the localized deformation [1–9], which is related to the grain structure and mobile dislocation density [1,2,10]. If the Lüders band cannot propagate over the specimen gage length, an early necking occurs and the specimen would fracture without uniform elongation [2,7]. In some cases where the Lüders band can propagate stably, a good combination of strength and ductility could be reached in ultrafine grained (UFG) materials [4,7–9,11]. The remarkable elongation is largely contributed by an unexpectedly huge Lüders strain, since necking is significantly postponed by stable propagation of Lüders band [12]. Lüders deformation is essentially caused by local plastic instability [7]. Lüders band is not desired because it affects the surface quality of metallic products during forming. Therefore, it is of practical interest to alleviate Lüders deformation.

Lüders deformation has been observed widely in low carbon steels [13,14], medium/high-Mn steels [4,15–17], IF steel [18], as well as in UFG pure metals [1,2]. In recent years, more attention has been paid to understanding the mechanism of large Lüders deformation, to the relationship between Lüders strain and grain size, grain structure and mobile dislocation density [1,2,8,19]. Only a few investigations have been focused on alleviating Lüders deformation in UFG materials without a dramatical loss of strength and ductility [16,20,21]. Here we report a heterostructure strategy on a recrystallized UFG-matrix 304-type metastable austenitic stainless steel to effectively avoid the discontinuous yielding without sacrificing much of the strength, and also to improve ductility (uniform elongation) and toughness.

2. Experimental procedures

The chemical composition of stainless steel is Fe-0.055C-0.40Si-1.63Mn-8.45Ni-17.30Cr (wt.%). After solution treatment at 1050 °C for 30 min, the as-received steel sheets with thickness of ~2.8 mm were cold rolled to ~0.56 mm in thickness at room temperature, and 0.05-0.1 mm reduction was carried out in each pass depending on the rolling

* Corresponding author. Nano and Heterogeneous Materials Center, School of Materials Science and Engineering, Nanjing University of Science and Technology, Nanjing, 210094, People's Republic of China.

** Corresponding author. Department of Materials Science & Engineering, City University of Hong Kong, Kowloon, 999077, Hong Kong, People's Republic of China.
E-mail addresses: jzliu@njust.edu.cn (J. Liu), y.zhu@cityu.edu.hk (Y. Zhu).

[1] The authors contributed equally to this work.

https://doi.org/10.1016/j.msea.2022.143393
Received 26 April 2022; Received in revised form 27 May 2022; Accepted 28 May 2022
Available online 31 May 2022

resistance. The ~80% thickness reduction resulted in a microstructure consisting of ~87% (in volume fraction) α'-martensite and 13% heavily deformed austenite. The cold-rolled specimens were then annealed at 650 °C for 30 min and 120 min, respectively, which produced two different recrystallized UFG microstructures. Microstructural characterization was carried out in a field-emission scanning electron microscope equipped with electron backscatter diffraction (EBSD) detector and an FEI T20 transmission electron microscope (TEM). Phase identification was conducted by X-ray diffraction (XRD) technique using Cu K_α radiation at room temperature (Smart Lab 9 kW), and the quantitative estimate details of martensite phase are described in the supplemental material. Tensile specimens with gauge dimensions of 25 mm × 6 mm were subjected to uniaxial and cyclic loading-unloading-reloading (LUR) tensile tests at room temperature (SANS CMT5105).

3. Results and discussion

Two typical recrystallized microstructures processed by cold rolling and annealing processes are shown in Fig. 1. After annealing at 650 °C for 30 min, specimen has a typical recrystallized microstructure composed of equiaxed ultrafine austenite grains with an average grain size of about 200 nm (Fig. 1a and i-1). This specimen is hereafter referred to as the UFG specimen. Annealing at the same temperature for 120 min produced a bi-modal heterostructure (HS) consisting of 30% (vol%) microcrystalline coarse grains (CGs) (1–4 μm) and 70% ultrafine grains as shown in Fig. 1d and i-2. Most of grains in the above two states have well-defined high-angle boundaries (HAGBs), and are almost free of dislocations (Fig. 1c and f). Some of the recrystallized grains contain annealing twins. The UFG structure was formed mostly from the reverse transformation of martensite [22], and partially from the recrystallization of heavily deformed austenite regions [23]. The coarse grains were formed through full recrystallization and grain growth due to the longer annealing time. Approximately 9% and 7% of α'-martensite phase are found retained in UFG and HS samples (Figs. 1b, 1e, and S1), respectively. This may be due to the relatively low annealing temperature, which makes reverse transformation from martensite to austenite incompletely [7]. The UFG and HS specimens have similar histogram distributions of grain boundary misorientation and kernel average misorientation (KAM), which makes it possible to isolate the effect of grain structure on their properties simplified.

The tensile behavior of the above UFG and HS steels are compared in Fig. 2a. Discontinuous yielding is observed in UFG steels, the tensile stress-strain curve showed a clear yield drop (from 1056 MPa to 1030 MPa) and a pronounced large Lüders strain (23%), which has been frequently reported in previous works [7–9,24]. The Lüders strain is approximate to 74% of the uniform elongation (UE, 31%) and 68% of

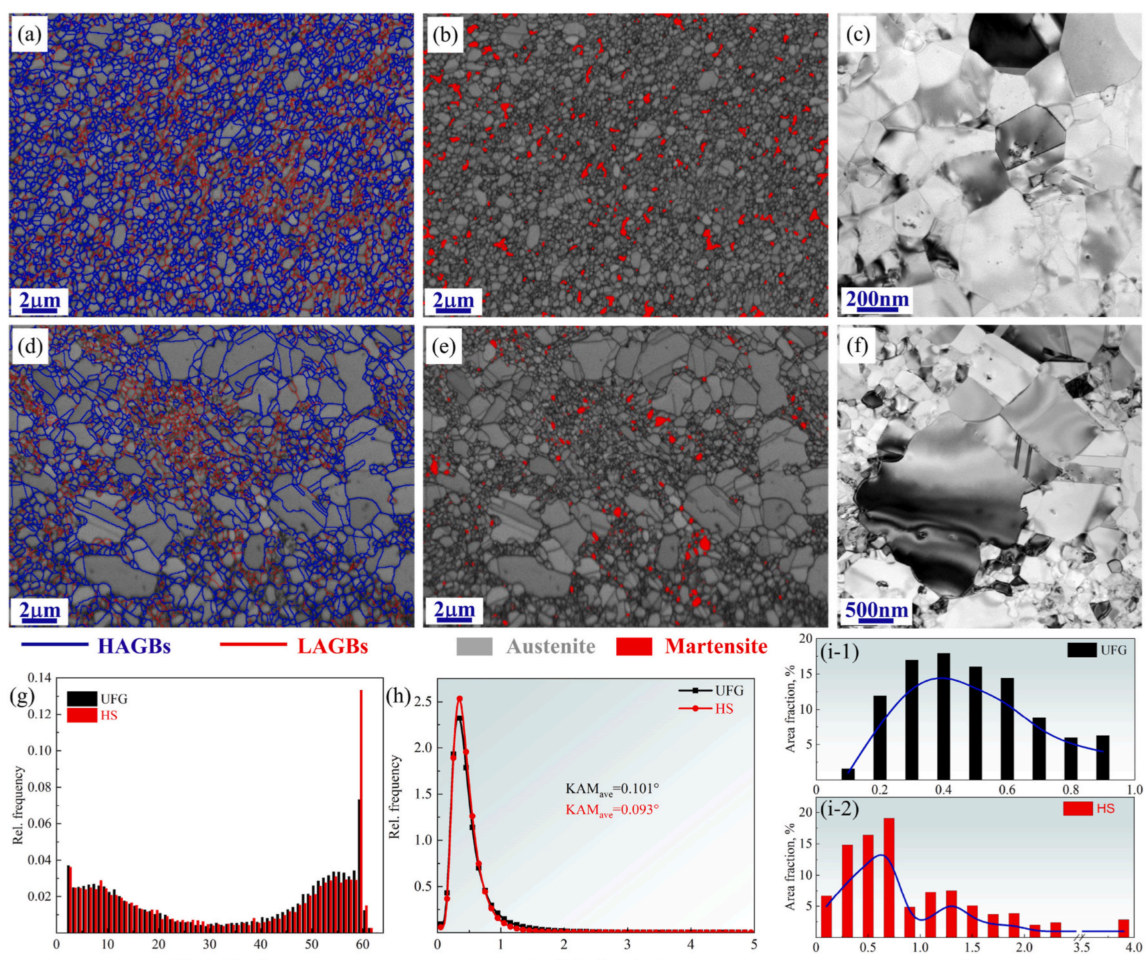

Fig. 1. Microstructural characteristics of ultrafine-grained (UFG) and bi-modal heterostructured (HS) steels. EBSD grain boundary images (a, d) and corresponding phase maps (b, e) of UFG (a, b) and HS samples (d, e). The red and blue lines in (a, d) represent low-angle grain boundaries (LAGBs, 2–15°) and high-angle grain boundaries (HAGBs, >15°), respectively. The untransformed martensite is marked by red color in (b, e). Typical TEM micrographs of UFG (c) and HS steels (f) showing defect-free austenite grains. Grain boundary misorientation distribution (g) and kernel average misorientation (KAM) distribution map (h) of experimental steels. (i-1) and (i-2) Grain size distribution of UFG and HS steels, respectively. (For interpretation of the references to color in this figure legend, the reader is referred to the Web version of this article.)

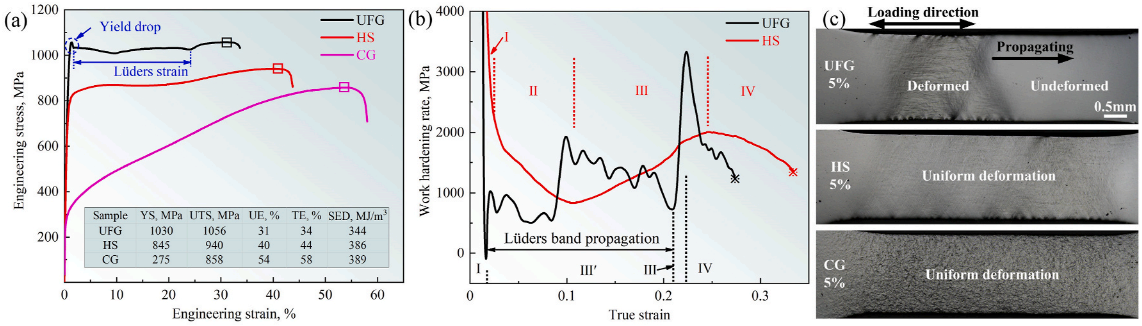

Fig. 2. (a) Engineering stress-strain curves of experimental steels with different initial microstructure, (b) corresponding work hardening rate plots, and (c) optical micrographs showing surface of tensile samples with a smaller gauge dimension of 2 mm in width and 5 mm in gage length. The inserted table in Fig. 2a shows the mechanical properties, where YS, UTS, UE, TE and SED are yield strength, ultimate tensile strength, uniform elongation, total elongation and strain energy density, respectively.

the total elongation (TE, 34%), respectively. After the stress plateau, slight strain hardening occurred, but the ultimate tensile strength (UTS) of 1056 MPa is soon reached at a strain of 31%, then necking occurred, which was followed by tensile failure. On the other hand, the HS steel showed a yield strength (YS) of 845 MPa, tensile strength of 940 MPa and a large total elongation of 44%. Apparently, the deformation behavior of the HS specimen is remarkably different from that of the UFG one. The HS specimens exhibit continuous yielding without a sudden stress drop and no Lüders deformation by regaining good strain-hardening capability. Its uniform elongation was increased to about 40%. The remarkable enhancement strain-hardening capability and ductility results in a notable gain in toughness (the strain energy density of 344 MJ/m^3 in UFG *vs.* 386 MJ/m^3 in HS *vs.* 389 MJ/m^3 in CG). Although the yield strength of HS steel became 18% lower than that of UFG one, it is still 3.1 times the strength of the CG sample.

The surfaces of tensile specimens after straining to ~5% were examined with an optical microscope. As shown in Fig. 2c, uniform deformation occurred in both the HS specimen and the CG specimen. While the UFG specimen shows a distinct strain localized region due to the formation of Lüders bands, which would gradually transform to the adjacent undeformed area with further straining. This provides the most direct proof that the Lüders deformation was suppressed effectively by bi-modal heterostructure.

The yield drop phenomenon in UFG steels is attributed to the suppression of intragranular Frank-Read sources and the activation of grain boundary dislocation sources [25–28]. The former reduces the number of mobile dislocations initially presented in the sample. The latter requires a greater nucleation stress to overcome an energy barrier, but can generate dislocations quickly once activated [1,29–31]. Thus, the recrystallized UFG specimen trend to lose the strain hardening quickly

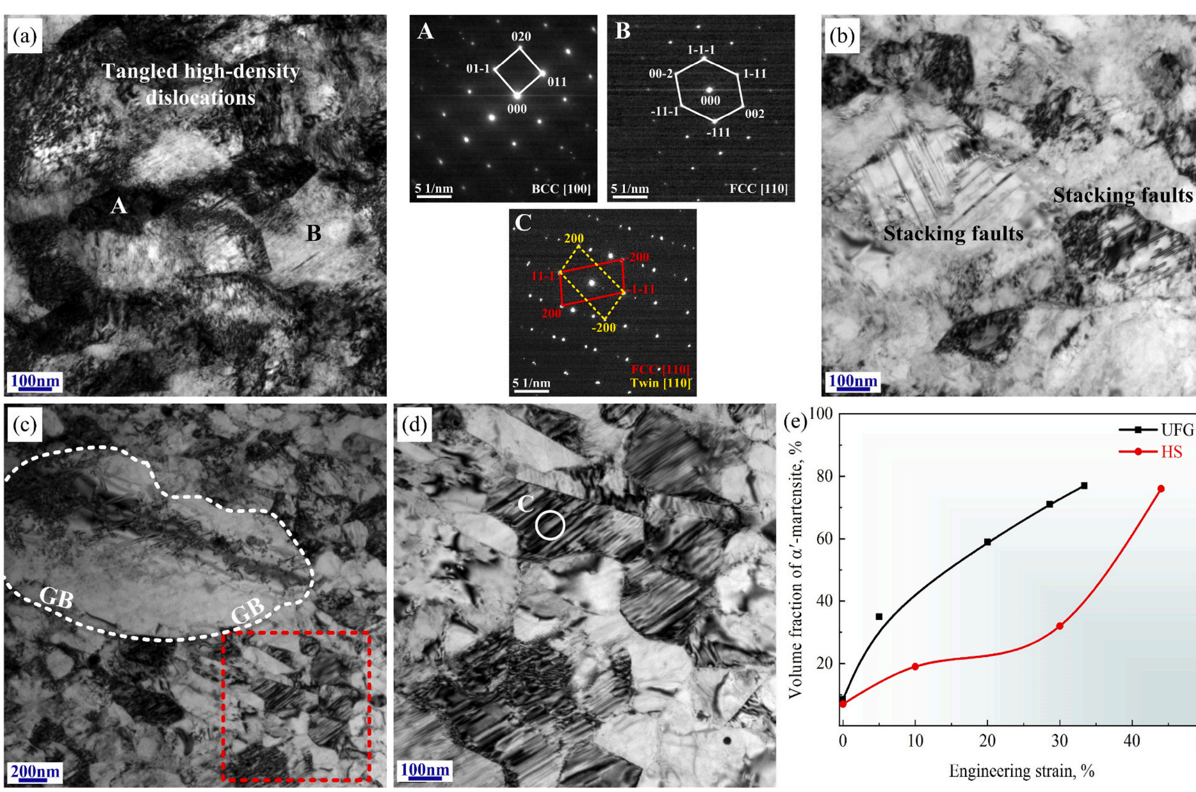

Fig. 3. Typical TEM micrographs of UFG steel at strain of ~0.05 (a and b) and HS steel after straining to ~0.095 (c and d). (a) Tangled high-density dislocations, (b) formation of stacking faults, (c) pile-up of GNDs in a coarse austenite grain (the white dash line refers the grain boundary) and (d) higher magnification image of area marked by red dashed lines in (c) showing typical features of UFG matrix near the soft coarse grain. (e) Volume fraction of α'-martensite as a function of strain. (For interpretation of the references to color in this figure legend, the reader is referred to the Web version of this article.)

on deformation owing to their very low dislocation storage ability inside grains [32]. The local stress near grain boundaries (GBs) is generally up to several times greater than that in the interior of grains [33,34], resulting in the activation of dislocation sources on grain boundaries [33,35]. The high density of GBs results in a large number of dislocation resources, thereby leading to a rapid increase in the density of dislocations (Fig. 3a) and stacking faults (Fig. 3b). The intersection sites of stacking faults are potential nucleation sites for the deformation-induced martensite [29], producing a rapid increase of martensite content (Fig. 3e) during the initial plastic deformation of the UFG specimens.

Thus, the stress concentration, due to the low initial mobile dislocation density, led to the initiation of Lüders bands; then stress relaxation occurred after the activation of dislocation sources at grain boundaries. The Lüders deformation followed, which was accompanied by rapid dislocation multiplication and martensitic transformation [7,29,36,37], making Lüders bands much stronger than the adjacent ultrafine austenite grains. This led to the nucleation and growth of new Lüders bands in adjacent regions. This process repeated itself as manifested by the fluctuation of strain hardening rate (stage III' in Fig. 2b), which finally produced a large Lüders strain [7,29].

As discussed above, the initiation of Lüders band is closely related to the limited strain-hardening capability, and high stress localization activating abundant dislocation sources at grain boundaries. Therefore, to avoid the Lüders deformation, we need to enhance the strain-hardening rate and promote strain delocalization. HS materials have been reported to promote dispersive strain localization to prevent the growth of Lüders bands [38–40]. Therefore, it is believed that the absence of Lüders deformation in the HS sample is due to the hetero-structure effect, i.e., by the introduction of a moderate population of micro-sized grains (soft) in UFG matrix (hard).

The deformation process of HS specimen differs fundamentally from that of its homogenous UFG and CG counterparts. With increasing applied strain, the soft CG zones yielded first while the UFG matrix remained elastic, i.e., intragranular Frank-Read dislocation sources in the CG grains were activated first at relatively low stresses. The plastic deformations of the CG zones were constrained by the surrounding UFG matrix. A high density of geometrically necessary dislocations (GNDs) is needed to accommodate the huge strain gradient in the hetero-boundary affected region (HBAR) in the CG zones [41], thereby elevating strain hardening rate, as shown in region II on the strain hardening rate-true strain curve of HS specimen (Fig. 2b). The GNDs accumulating within soft CGs (Fig. 3c) produce hetero-deformation induced (HDI) strengthening. As a result, the CG zones are significantly strengthened [33,42].

As shown in Fig. 3e (Fig. S2 gives the corresponding XRD patterns), compared with the UFG specimens, the martensitic transformation is severely suppressed in the HS specimens, instead, a high density of deformation twins was observed (Fig. 3d). This is because the critical stress to activate twinning (~750 MPa in our case) is lower than that for martensitic transformation (approximately equals to the upper yield point of 1056 MPa) in ultrafine austenite grains [43,44] (see the details in the supplemental material). The twin boundaries (TBs) can act as strong barriers to dislocation motion, dislocations pileup at the TBs, which enhances strain hardening (region IV on the strain hardening rate-true strain curve of HS specimen in Fig. 2b). This led to a dramatical increase of martensite (from 31% to 76% at the strain from 30% to 44% in Fig. 3e), resulting from dislocation and twin substructures with high localized plastic strain [8].

The HDI strengthening and HDI strain hardening has been verified to be an unique strengthening and toughening mechanism in HS metallic materials [38,39,41], which can be evaluated quantitatively from the LUR hysteresis loops (Fig. 4a). The partition of HDI stress (σ_{HDI}) and effective stress (σ_{eff}) is schematically illustrated in Fig. 4b, and those stresses can be expressed by the following equations according to the method introduced by Dickson et al. [45].

$$\sigma_{eff} = \frac{\sigma_0 - \sigma_u}{2} + \frac{\sigma^*}{2} \tag{1}$$

$$\sigma_{HDI} = \sigma_0 - \sigma_{eff} \tag{2}$$

where σ_0 (point P_0) is the maximum flow stress prior to unloading, σ^* is the thermal component of the stress corresponding to the quasi-elastic segment P_0P_1, and σ_u (point P_3) is the unloading yield stress, which is deviated from the elastic limit P_2 with a plastic strain offset equal to 0.1%.

Although the hysteresis loops for UFG steel are as plump as that for HS specimen, remarkable yield drop can be observed from the LUR tensile curves of UFG sample (Fig. 4a). This must be related to the Lüders banding in UFG steel. However, it must be admitted that the physical meaning of the unloading stress-strain curve during Lüders deformation is still not clear, and thus maybe it does not make sense that the measurement of HDI stress in UFG samples with Lüders-like deformation.

For HS steels, both the HDI stress and the effective stress increase constantly, as shown in Fig. 4c, which produced an enhanced strain hardening capability, resulting in a good toughness. The HDI strengthening and HDI strain hardening significantly enhanced the strength and toughness of the HS specimen. The effective stress evolution can be interpreted as flow stress caused by total dislocation density [46,47]. The HDI stress is a long-range internal stress caused by GND pile-ups [40]. The high HDI stress could also be produced by extremely high density of GBs [48] and phase boundaries [17], despite of the limitation on the length of each pile-up. In addition, this could also be caused by the martensitic transformation, which itself could produce the HDI stress because dislocations are involved in the nucleation and growth of martensite. However, The HDI stress evolution caused by the transformation induced plasticity (TRIP) observed here is not well understood, and need to be systematically studied in the future.

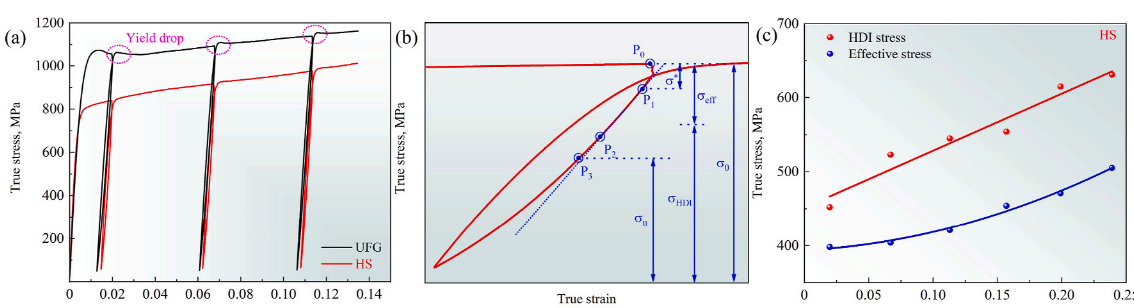

Fig. 4. Estimates of the HDI stress and effective stress contributions during LUR tests. (a) Hysteresis behavior of UFG and HS steels during LUR tensile tests. (b) Schematic illustration of the partition of HDI stress (σ_{HDI}) and effective stress (σ_{eff}) in unloading half cycle. (c) Evolution of those stress components with strain of HS steel.

4. Conclusion

In summary, our approach to introduce moderate population of micron-sized grains in UFG matrix can effectively alleviate the Lüders deformation of the UFG 304 stainless steel, and at the same time retained high strength and enhanced ductility and toughness. The Lüders-type deformation is closely associated with the deformation-induced martensitic transformation occurring in homogenous UFG stainless steel. Both the plastic deformation of CGs under multi-axial stress states and the activation of twining in UFG regions by HDI strengthening, greatly enhanced the strain hardening capability of HS stainless steel. The strain delocalization and the enhanced strain hardening capability are responsible for the effective suppression of Lüders-type deformation.

Originality Statement

I write on behalf of myself and all co-authors to confirm that the results reported in the manuscript are original and neither the entire work, nor any of its parts have been previously published. The authors confirm that the article has not been submitted to peer review, nor has been accepted for publishing in another journal. The author(s) confirms that the research in their work is original, and that all the data given in the article are real and authentic. If necessary, the article can be recalled, and errors corrected.

CRediT authorship contribution statement

Guosheng Sun: Conceptualization, Data curation, Formal analysis, Investigation, Writing – original draft, Writing – review & editing, Funding acquisition. **Jizi Liu:** Conceptualization, Formal analysis, Investigation, Writing – review & editing, Funding acquisition. **Yuntian Zhu:** Conceptualization, Writing – review & editing, Funding acquisition.

Declaration of competing interest

The authors declare that they have no known competing financial interests or personal relationships that could have appeared to influence the work reported in this paper.

Acknowledgments

This work was supported by the Postdoctoral Research Foundation of China (Grant 2020M681602), the Jiangsu Postdoctoral Research Foundation (Grant 2020Z259) and the Natural Science Foundation of Jiangsu Province (Grant. BK20201308). The authors are thankful for the technical support from the Jiangsu Key Laboratory of Advanced Micro & Nano Materials and Technology, the Analysis and Test Center of Nanjing University of Science and Technology, and the Hong Kong Research Grants Council (GRF 11214121).

Appendix A. Supplementary data

Supplementary data to this article can be found online at https://doi.org/10.1016/j.msea.2022.143393.

References

[1] C.Y. Yu, P.W. Kao, C.P. Chang, Acta Mater. 53 (2005) 4019–4028.
[2] Y.Z. Tian, S. Gao, L.J. Zhao, S. Lu, R. Pippan, Z.F. Zhang, N. Tsuji, Scripta Mater. 142 (2018) 88–91.
[3] Y. Tomata, A. Narui, N. Tsuchida, ISIJ Int. 48 (2008) 1107–1113.
[4] B.B. He, B. Hu, H.W. Yen, G.J. Cheng, Z.K. Wang, H.W. Luo, M.X. Huang, Science 357 (2017) 1029–1032.
[5] X.G. Wang, L. Wang, M.X. Huang, Acta Mater. 124 (2017) 17–29.
[6] M.Z. Zhang, R.G. Li, J. Ding, H.Y. Chen, J.S. Park, J. Almer, Y.D. Wang, Mater. Res. Lett. 6 (2018) 662–667.
[7] S. Gao, Y. Bai, R. X Zheng, T.Z. Tian, W.Q. Mao, A. Shibata, N. Tsuji, Scripta Mater. 159 (2019) 28–32.
[8] C.X. Huang, G. Yang, C. Wang, Z.F. Zhang, S.D. Wu, Metall. Mater. Trans. A 42 (2011) 2061–2071.
[9] G.S. Sun, M.M. Zhao, L.X. Du, H.Y. Wu, Mater. Char. 184 (2022), 111674.
[10] J. Han, S.J. Lee, J.G. Jung, Y.K. Lee, Acta Mater. 78 (2014) 369–377.
[11] Y. Zhang, H. Ding, Mater. Sci. Eng., A 733 (2018) 220–223.
[12] J. Han, S.H. Kang, S.J. Lee, Y.K. Lee, J. Alloys Compd. 681 (2016) 580–588.
[13] M.S. Mohsenzadeh, M. Mazinani, Mater. Sci. Eng., A 673 (2016) 193–203.
[14] N. Tsuchida, H. Masuda, Y. Harada, K. Fukaura, Y. Tomota, K. Nagai, Mater. Sci. Eng., A 488 (2008) 446–452.
[15] C.Y. Hung, Y. Bai, N. Tsuji, M. Murayama, J. Mater. Sci. Technol. 86 (2021) 192–203.
[16] K. Steineder, D. Krizan, R. Schneider, C. Béal, C. Sommitsch, Acta Mater. 139 (2017) 39–50.
[17] X.H. Wan, G. Liu, Z.G. Yang, H. Chen, Scripta Mater. 198 (2021), 113819.
[18] S. Gao, M.C. Chen, M. Joshi, A. Shibata, N. Tsuji, J. Mater. Sci. 49 (2014) 6536–6542.
[19] Z.H. Cai, S.Y. Jing, H.Y. Li, K.M. Zhang, R.D.K. Misra, H. Ding, Z.Y. Tang, Mater. Sci. Eng., A 739 (2019) 17–25.
[20] Z.C. Li, H. Ding, R.D.K. Misra, Z.H. Cai, Mater. Sci. Eng., A 679 (2017) 230–239.
[21] S. Yan, T.L. Li, T.S. Liang, J.Q. Chen, Y. Zhao, X.H. Liu, Mater. Sci. Eng., A 758 (2019) 79–85.
[22] C.S. Lei, X.L. Li, X.T. Deng, Z.D. Wang, Metall. Mater. Trans. A 49 (2018) 6134–6146.
[23] G.S. Sun, L.X. Du, J. Hu, R.D.K. Misra, Mater. Sci. Eng., A 709 (2018) 254–264.
[24] G. Niu, H.S. Zurob, R.D.K. Misra, Q.B. Tang, Z.H. Zhang, M.T. Nguyen, L.L. Wang, H.B. Wu, Y. Zou, Acta Mater. 226 (2022), 117642.
[25] D.E. Spearot, M.A. Tschopp, K.I. Jacob, D.L. McDowell, Acta Mater. 55 (2007), 705714.
[26] M. Kato, Mater. Sci. Eng., A 516 (2009), 276282.
[27] T. Shimokawa, Phys. Rev. B 82 (2010), 174122.
[28] T. Shimokawa, S. Kitada, Mater. Trans. 55 (2014) 58–63.
[29] R.S. Varanasi, S. Zaefferer, B.H. Sun, D. Ponge, Mater. Sci. Eng., A 824 (2021), 141816.
[30] J.P. Hirth, Metall. Trans. A 3 (1972) 3047–3067.
[31] L. Capolungo, D.E. Spearot, M. Cherkaoui, D.L. McDowell, J. Qu, K.I. Jacob, J. Mech. Phys. Solid. 55 (2007) 2300–2327.
[32] Y.M. Wang, E. Ma, Mater. Sci. Eng., A 375–377 (2004) 46–52.
[33] H. Wu, G.H. Fan, Prog. Mater. Sci. 113 (2020), 100675.
[34] G. Martin, C.W. Sinclair, J.H. Schmitt, Scripta Mater. 68 (2013) 695–698.
[35] K.R. Magid, J.N. Florando, D.H. Lassila, M.M. LeBlanc, N. Tamura, J.W. Morris, Philos. Mag. A 89 (2009) 77–107.
[36] X.X. Huang, N. Hansen, N. Tsuji, Science 312 (2006) 249–251.
[37] G.T. Hahn, Acta Metall. 10 (1962) 727–738.
[38] Y.F. Wang, C.X. Huang, Y.S. Li, F.J. Guo, Q. He, L.Y. Song, X.L. Wu, R. O. Scattergood, Y.T. Zhu, Int. J. Plast. 124 (2020) 186–198.
[39] Y.F. Wang, C.X. Huang, Q. He, F.J. Guo, M.S. Wang, L.Y. Song, Y.T. Zhu, Scripta Mater. 170 (2019) 76–80.
[40] Y.T. Zhu, K. Ameyama, P.M. Anderson, I.J. Beyerlein, H.J. Gao, H.S. Kim, E. J. Lavernia, S.N. Mathaudhu, H. Maghrabi, R.O. Ritchie, N. Tsuji, X.Y. Zhang, X. L. Wu, Mater. Res. Lett. 9 (2021) 1–30.
[41] X.L. Wu, Y.T. Zhu, MRS Bull. 46 (2021) 244–249.
[42] M.Y. Seok, J.A. Lee, D.H. Lee, U. Ramamurty, S. Nambu, T. Koseki, J. Jang, Acta Mater. 121 (2016) 164–172.
[43] T.S. Byun, Acta Mater. 51 (2003) 3063–3071.
[44] A. Weidner, K. Fischer, H. Biermann, Mater. Sci. Eng., A 799 (2021), 140197.
[45] J.L. Dickson, J. Boutin, L. Handfield, Mater. Sci. Eng. 64 (1984) 7–11.
[46] X. Feaugas, Acta Mater. 47 (1999) 3617–3632.
[47] X.L. Wu, M.X. Yang, F.P. Yuan, G.L. Wu, Y.J. Wei, X.X. Huang, Y.T. Zhu, Proc. Natl. Acad. Sci. U.S.A. 112 (2015) 14501–14505.
[48] Y.F. Wang, M.X. Yang, X.L. Ma, M.S. Wang, K. Yin, A.H. Huang, C.X. Huang, Mater. Sci. Eng., A 727 (2018) 113–118.